Journal of Molecular Catalysis A: Chemical 366 (2013) 109–115

Contents lists available at SciVerse ScienceDirect

Journal of Molecular Catalysis A: Chemical

journal homepage: www.elsevier.com/locate/molcata

Catalysts based on Rh(III)-hexamolybdate/γ-Al_2O_3 and their application in the selective hydrogenation of cinnamaldehyde to hydrocinnamaldehyde

Guillermo R. Bertolini[a], Carmen I. Cabello[a,b,*], Mercedes Muñoz[a], Mónica Casella[a], Delia Gazzoli[c], Ida Pettiti[c], Giovanni Ferraris[c]

[a] "Centro de Investigación y Desarrollo en Ciencias Aplicadas Dr. J. Ronco" (CINDECA-CCT CONICET La Plata – Universidad Nacional de La Plata), Calle 47 No. 257, 1900 La Plata, Argentina
[b] Facultad de Ingeniería UNLP and Member CICPBA, Argentina
[c] "Dipartimento di Chimica" La Sapienza Università di Roma, Piazzale Aldo Moro 5, I-00185 Roma, Italy

ARTICLE INFO

Article history:
Received 14 December 2011
Received in revised form
13 September 2012
Accepted 14 September 2012
Available online 25 September 2012

Keywords:
Heteropolyoxomolybdates
Anderson phases of Rh(III)
$RhMo_6/\gamma\text{-}Al_2O_3$
Cinnamaldehyde
Selective hydrogenation
Hydrocinnamaldehyde

ABSTRACT

Several catalysts based on $[RhMo_6O_{24}H_6]^{3-}$ ($RhMo_6$) heteropolyanion supported on γ-Al_2O_3 with different textural properties were prepared, characterized and tested in the liquid-phase hydrogenation of cinnamaldehyde. The characterization of pure and supported systems was carried out using several techniques including XRD, SEM-EDS microscopy, Raman microprobe, X-ray photoelectron spectroscopies and temperature programmed reduction (TPR). The catalytic performance was monitored by conversion of the starting cinnamaldehyde as a function of time: the initial activities represented as the turnover frequency (TOF), were measured considering the surface Rh atoms. The planar heteropolyanion $RhMo_6$/(EI) based systems showed enhanced catalytic activity over the RhMo conventional catalyst obtained by successive impregnation of both transition metal ions (Rh(III) chloride and heptamolybdate). The selectivity for the $RhMo_6$ systems was mainly toward HCAL unlike the conventional catalyst which showed selectivity toward CA. This study also showed a synergetic effect between Rh and Mo through which Rh promoted Mo reducibility.

1. Introduction

The selective hydrogenation of α,β-unsaturated aldehydes assisted by supported metal catalysts is a key stage in the preparation of pharmaceutical products, flavors and fragrances [1–3]. The selective hydrogenation of cinnamaldehyde (CAL) is a good example of this commercially important reaction that allows the attainment of cinnamic alcohol (CA), hydrocinnamaldehyde (HCAL) and 3-phenyl propanol (PP). The cinnamic alcohol is a valuable product in the perfume industry for its aroma as well as for its fixation properties. Also, it is used in the pharmaceutical industry in the synthesis of chloromycetin antibiotic [4,5]. More recently, important applications were found for the hydrocinnamaldehyde used as intermediate in the synthesis of medicines for the treatment of HIV [6–8].

The hydrogenation process is a complex one when the molecule to be hydrogenated has two or more functional groups of comparable reactivity. This situation is present in molecules that have C=C and C=O conjugated groups such as α,β-unsaturated aldehydes or ketones. An example is the selective hydrogenation of cinnamaldehyde (CAL) [9–12]. This species is a vinylic derived of benzaldehyde and the aldehyde group behaves with catalyst as if it were an aromatic aldehyde. The carbonyl group is reduced easily and competes with saturation of the C=C double bond [13]. The hydrogenation of CAL catalyzed by supported noble metals leads usually to a mixture of HCAL, CA and PP. The selectivity to CA is highly dependent on the nature of the precious metal used as catalyst [14], and the noble metals selectivity can be classified in the following sequence: Pd < Rh < Ru < Pt < Ir. Pd and Rh generally display high activity but rather poor selectivity toward cinnamyl alcohol and during the past few years, several examples of synthesis and properties of mono or bi metallic Pd catalysts for selective hydrogenation of CAL to HCAL have been reported [15–17]. Little has been published concerning the use of rhodium for the selective hydrogenation of CAL to HCAL. Additionally, it was found that the catalysts deactivation rate in monometallic systems is significant and hence a low stability derives [18]. Therefore, in the hydrogenation field, bimetallic catalysts are often used in order to improve selectivity and stability of a single component catalyst [19,20]. In general, supported bimetallic catalysts are very interesting materials because one metal can tune and/or modify the catalytic properties of the other metal as a result of both electronic and structural effects [20,21]. In this

* Corresponding author: Tel.: +54 221 4210711; fax: +54 221 4210711.
E-mail address: ccabello@quimica.unlp.edu.ar (C.I. Cabello).

1381-1169/$ – see front matter © 2012 Elsevier B.V. All rights reserved.
http://dx.doi.org/10.1016/j.molcata.2012.09.013

sense, bi- or trimetallic catalytic systems based on heteropolyacids or polymetalates (HPOMs), both as bulk and supported systems, have started to replace a large number of conventional oxide precursors, improving the efficiency and environmental conditions of several catalytic processes [22].

Our recent studies have shown that Co, Ni or Rh containing heteropolymolybdates with Anderson-type structure are interesting precursors in heterogeneous catalysts for hydrotreatment processes [23,24]. Such studies have shown that the planar structure of the heteropolyoxoanion as well as its redox and solubility properties are relevant factors in the heteropolyanion-support interaction, producing an active surface with an ordered distribution and uniform deposition of the metallic elements, which favors the synergic effect.

In continuation of our studies of these phases as bimetallic catalytic precursors, in the present paper we have studied the selective hydrogenation of CAL by using catalysts based on Anderson-type heteropolyoxometalates with formula $(NH_4)_3[RhMo_6O_{24}H_6]\cdot 7H_2O$ supported on γ-Al_2O_3. The $RhMo_6$/γ-Al_2O_3 systems resulted active and selective for the hydrogenation of CAL to HCAL and their performance were compared with those of a conventional RhMo/γ-Al_2O_3 catalyst, prepared by successive impregnation.

2. Experimental

2.1. Catalyst preparation

The synthesis of the precursor with formula $(NH_4)_3[RhMo_6O_{24}H_6]\cdot 7H_2O$ ($RhMo_6$) was carried out from the aqueous solution reaction of ammonium heptamolybdate and $RhCl_3\cdot 6H_2O$ in stoichiometric proportions, as previously reported [23,24].

In order to analyze the support effect, we selected an alumina support thermally treated at 773 K in air for 24 h (hereafter B) and two types of commercial γ-Al_2O_3 spheralite, hereafter EI and EII from YPF Oil Company (Yacimientos Petrolíferos Fiscales Argentina). The procedure adopted for the catalyst preparation was the equilibrium adsorption impregnation using heteropolymolybdate aqueous solution prepared as previously reported [24,25]. The $RhMo_6$ catalysts were obtained by adding 10 mg Mo/mL of $RhMo_6$ aqueous solution to γ-Al_2O_3 (EI and EII types) and Al_2O_3 (B) supports to obtain catalysts with ca. Mo 6 wt% and Rh 1 wt%, and drying at 353 K. The resulting samples were labeled $RhMo_6$/E(I), $RhMo_6$/E(II) and $RhMo_6$/(B), respectively.

A conventional RhMo catalyst was prepared by successive impregnation of type (B) alumina, in excess of pore volume. According to a literature method [21] this catalyst was obtained by first adding the $RhCl_3\cdot 6H_2O$ solution to the support and drying at 353 K. The solid was then impregnated with a $(NH_4)_6[Mo_7O_{24}]\cdot 4H_2O$ (AHM) solution and dried at 353 K. The resulting sample, containing 6% of Mo and 1% of Rh, was labeled RhMo/(B).

Before the catalytic tests, all catalysts were pretreated in a flow of H_2, at 623 K, for 2 h.

2.2. Chemical analysis

The Mo and Rh content was determined by atomic absorption spectrometry (AAS), using an IL-457 spectrometer, on initial (C_i) and final (C_f) solutions. The Mo and Rh adsorbed concentrations (C_a^{Mo} or C_a^{Rh}) were calculated from experimental C_i (initial) and C_f (final) data, taking into account the volume of the impregnated solution and the support mass (mass balance) according to the expression:

$$C_a = \left\{ \frac{(C_i - C_f \times V)}{m} \right\} \times 100.$$

2.3. Characterization of catalysts

X-ray powder diffraction patterns were recorded in the 2θ angular range from 5° to 70° by a diffractometer Philips PW 1714 using Cu Kα radiation (Ni filter).

Scanning electron microscopy (SEM) with EDS analysis was performed by a Microscope Philips SEM 505 with dispersive energy system for microanalysis, EDAX 9100.

Raman spectra were collected on powder samples at room temperature in the back-scattering geometry with an in Via Renishaw spectrometer equipped with an air-cooled CCD detector and a super-Notch filter. The emission line at 514.5 nm from an Ar^+ ion laser was focused on the sample under a Leica DLML microscope using a 20× objective. Five 20-s accumulations were attained for each sample with an incident beam power of about 5 mW. The spectral resolution was 2 cm^{-1} and the spectra were calibrated using the 520.5 cm^{-1} line of a silicon wafer.

XPS spectra were measured on a Leybold–Heraeus LHS10 spectrometer in FAT mode (50 eV pass energy) with Mg Kα radiation (12 kV, 20 mA) at a pressure lower than 10^{-9} Torr. The samples, manually pressed onto a gold plate, were analyzed as prepared and after treatment in H_2 outside the spectrometer. The Rh3d, Mo3d, O1s, C1s and Al2p regions were processed by computer. Electron binding energies were referenced to the C1s peak at 285.0 eV. The intensity ratios, I_{Me}/I_{Al}, (Me = Rh or Mo) were obtained from peak area determination by integration of the appropriate peak after smoothing and nonlinear Shirley-type background subtraction by Esca Tools 4.2 software (Surface Interface, Inc., Mountain View, CA). To assess a quantitative relationship between the XPS peak intensity ratio and surface composition, the experimental results were compared with the values predicted by the sensitivity factor, S, approach firstly proposed by Wagner et al. [26].

Surface area measurements, Brunauer–Emmett–Teller (BET) [27] multipoint method, and textural analysis were obtained using a Micromeritics ASAP 2020 equipment. The samples were pretreated under vacuum in two stages of 1 h at 373 and 573 K. The pore distribution was determined by the Barret–Joyner–Halenda (BJH) method [28] from the analysis of micropore isotherm by the t-test [29] taking the curve of Harkins and Jura [30]; the total pore volume was determined by the rule of Gurvitsch [31].

The temperature programmed reduction (TPR) diagrams were obtained in a flow system with a mixture of 10% volume H_2 and 90% N_2 volume (20 cm^3/min), by heating from room temperature up 1123 K at 10 K/min with a Quantasorb Jr. (Quantachrome) equipment.

Measurements of Rh dispersion were made following the Boudart method: Rh dispersion, defined as the ratio of the exposed Rh atoms to the number of total Rh atoms, was determined by H_2/O_2 titration [32] using a volumetric apparatus. The fresh samples (typically 0.5–1 g, depending on Rh content) were pretreated in flowing N_2 at 423 K for 30 min, reduced in H_2 (10% in He) at 623 K for 1 h and then purged with N_2 at 623 K for 1 h before cooling down to RT in N_2. Samples were then exposed to O_2 (10% in N_2) at RT for 30 min, and flushed with N_2 for 30 min at RT. After careful evacuation at RT down to 1 Pa, the irreversibly adsorbed H_2 at RT, H_{irr}, was determined. In particular, total H_2 uptakes were determined by zero pressure extrapolation of the adsorption isotherm, usually in the hydrogen pressure range 6.6–26.6 kPa. Samples were subsequently evacuated at RT for 0.5 h and a second isotherm due to the reversible part of the adsorption was determined. The difference between the total (first isotherm) and the reversible (second isotherm) uptakes in the parallel and linear part of the isotherms gave the irreversible part of the adsorption (double isotherm method). The exposed Rh atoms, Rh_s, were then calculated from H_{irr} (irr = irreversible), assuming a H_{irr}/Rh_s ratio of 1 and by taking into account the

overall stoichiometry: $Rh_s—O + 3/2\ H_2 = Rh_s—H_{irr} + H_2O$. Finally the Rh dispersion, D, was calculated as H_{irr}/Rh_{tot}.

2.4. Catalytic test

All catalysts were pretreated in H_2 atmosphere at 623 K for 2 h to achieve the reduction of metallic ions.

The hydrogenation reaction in liquid phase was performed in an Autoclave Engineers reactor provided with a stirrer (500 rpm). The reaction was performed under kinetic regime at 358 K with a cinnamaldehyde concentration of 0.1 mol/L and a H_2 pressure of 10 bar, using 0.2 g of pretreated catalyst. The cinnamaldehyde was introduced in the reactor dissolved in 60 mL of toluene. The reaction progress was monitored by taking a series of micro samples, which were analyzed chromatographically by Varian 3400 CX equipment provided with a capillary column Megabore DB-WAX and a flame ionization detector. At the same time, complementary measurements were made with a spectrometer CG/EM Q-mass 910.

The % CAL conversion was calculated from the difference between initial CAL moles and CAL moles not consumed in a time t/initial CAL moles.

The selectivity (%) was calculated based on the ratio product moles/total moles of obtained products.

TOF_{Rhsurf} (turnover frequencies) numbers were calculated by the [CAL] $\mu mol\ s^{-1}$/surface Rh atoms equation from initial rate of CAL conversion vs. time (from $t = 0$ to 50 min of reaction). Data of Rh dispersion as H_{irr}/Rh_{tot} were previously obtained by the above-described Boudart method [32].

3. Results and discussion

3.1. Precursor and catalyst characterization

SEM-EDS microscopy showed that the synthesized crystals of $(NH_4)_3[RhMo_6O_{24}H_6]\cdot 7H_2O$ ($RhMo_6$) (pale orange) were similar to other Anderson phases widely studied in our laboratory such as $CoMo_6$, $CrMo_6$ and $AlMo_6$ [24]. The XRD pattern on powder samples also demonstrated that the Rh phase was isomorphous to phases containing a trivalent metal as heteroatom [23–25]. The polyhedral structure of Rh(III) hexamolybdate of formula $[RhMo_6O_{24}H_6]^{3-}$, with planar D_{3d} symmetry, is constituted by Rh(III) as heteroatom in the center of an octahedron whose corners are (OH) groups shared with six Mo(VI)O_6 octahedrons (Fig. 1(a)). The structure of the heptamolybdate isopolyanion, formed by seven octahedrons Mo(VI)O_6 in anion planar configuration, is shown comparatively in Fig. 1(b).

All catalysts prepared by both equilibrium adsorption and successive impregnation methods contained about 6 wt% Mo and 1 wt% Rh. As demonstrated in our previous work, the adsorption process of $RhMo_6$ responded to a Langmuir-type adsorption isotherm as for all XMo_6 phases [24]. We have previously shown that on γ-Al_2O_3 spheralite (EI) [24,25] the heteropolyanion adsorption depends strongly on the heteroatom. The adsorption constant, K_{ad}, varies according to the following order: $RhMo_6 > CrMo_6 > CoMo_6 > TeMo_6–AlMo_6 > NiMo_6 \gg$ AHM [24,25]. The K_{ad} resulted several orders of magnitude higher than those of AHM, and this was explained not only by the planar heteropolyanion structure but also by the heteroatom (X) type. All these factors indicated that in the first impregnation step, a series of homogeneous and heterogeneous processes in equilibrium occurred involving the phase deposition and some secondary reactions. These reactions, including the Al dissolution of the support, counter diffusion and exchange of cations, have already been characterized by spectroscopic and thermal methods [24].

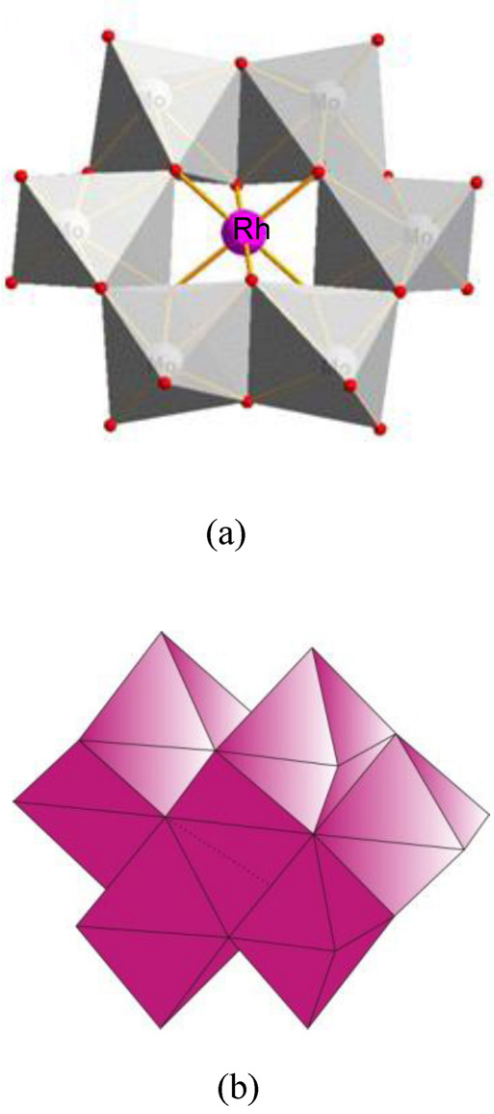

Fig. 1. Representation of structures corresponding to: (a) planar heteropolyanion Rh(III) hexamolybdate $[RhMo_6O_{24}H_6]^{3-}$ and (b) isopolyanion heptamolybdate $[Mo_7O_{24}]^{6-}$.

The XRD analysis of pretreated $RhMo_6$ catalysts supported on spheralite-type alumina (EI and EII) showed the presence of γ-Al_2O_3 (ASTM: 89-7717), Fig. 2, curve a. The XRD pattern of both pretreated $RhMo_6$ and RhMo catalysts on support B showed lines corresponding to α-AlO(OH) (boehmite, ASTM-83-2384) and emerging peaks from γ-Al_2O_3 (Fig. 2, curve b). However, all the patterns of supported catalysts showed no lines other than those of the supports, indicating spreading of different structures containing Rh and Mo.

The textural analysis of the supports, Table 1, indicated that support B had lower surface area and pore volume values than E(I) and E(II) supports. The pore size distribution of the supports, Fig. 3, reveals that the higher surface area of E(II) with respect to those measured for E(I) and γ-Al_2O_3 B (319 $m^2\ g^{-1}$ vs. 255 and

Table 1
Textural parameters of different alumina supports.

Support type	SBET ($m^2\ g^{-1}$)	Pore volume ($cm^3\ g^{-1}$)
(B) Al_2O_3 ($T = 500\ ^\circ C$)	149	0.23
(EI) γ-Al_2O_3 Spheralite I	255	0.65
(EII) γ-Al_2O_3 Spheralite II	319	0.36

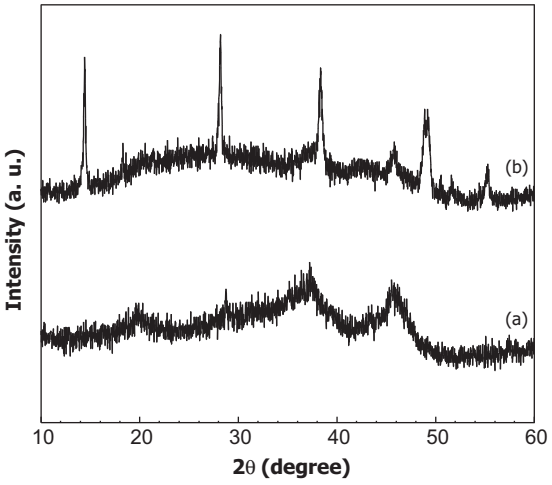

Fig. 2. XRD pattern of pretreated supported $RhMo_6$ catalysts: (a) $RhMo_6/\gamma\text{-}Al_2O_3$ spheralite E(I) or E(II); (b) RhMo or $RhMo_6/Al_2O_3$(B).

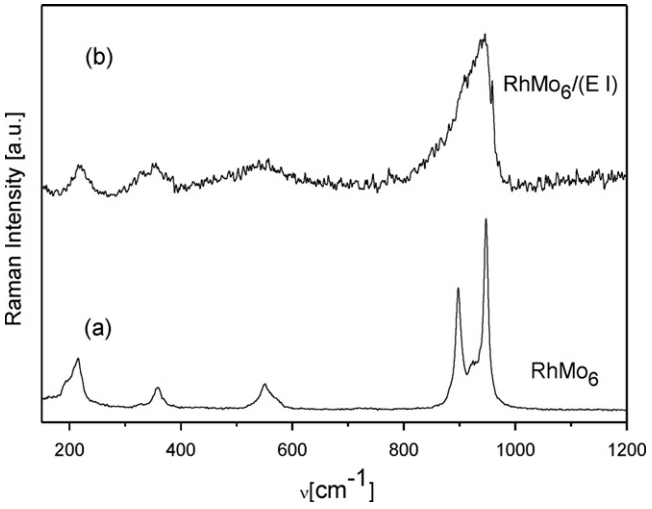

Fig. 4. Raman spectra: (a) $(NH_4)_3[RhMo_6O_{24}H_6]\cdot 7H_2O$ ($RhMo_6$) and (b) $RhMo_6$/E(I).

$149\,m^2\,g^{-1}$, respectively), may be assigned to the higher fraction of narrow mesopores and/or micropores (i.e. pores around and below 30 Å in average diameter) present in this support.

The identification of molecular structures, such as those of iso and heteropolyoxomolybdates characterized by Mo—O—X and Mo—O—Mo bridges and terminal Mo=O bonds, can easily be accomplished by Raman spectroscopy [33].

By comparing the Raman spectrum of the $RhMo_6$ precursor (Fig. 4, curve a) with that of $RhMo_6/\gamma\text{-}Al_2O_3$ [E(I)] fresh catalyst (Fig. 4, curve b), it is evident that the interaction of the Anderson phase with the support yielded band broadening and shift to lower frequencies in agreement with previously published results [33]. In fact, the sharp bands, typical of Anderson structure, associated with the symmetric stretching mode of terminal $Mo—O_{2t}$ bonds at $949\,cm^{-1}$ (ν_s) and the antisymmetric stretching at 889 and $852\,cm^{-1}$ (ν_{as}), merged into an unresolved feature. A different behavior was observed for the fresh catalysts prepared by successive impregnation of the support with rhodium chloride and AHM aqueous solutions.

The comparison of the Raman features of AHM (Fig. 5, curve a) with those of the RhMo/(B) catalyst (Fig. 5, curve b) shows that the symmetric stretching mode MoO_{2t} at $934\,cm^{-1}$ of the heptamolybdate species broadened and shifted to higher frequencies ($947\,cm^{-1}$), which is indicative of a change in the structure of the supported isopolyanion. It is well known that during impregnation of the alumina support with an aqueous AHM solution, precipitation of the hexamolybdoaluminate of Anderson-type structure ($AlMo_6$) occurs due to the extraction of Al atoms from the alumina surface [34]. The presence of a broad band around $540\,cm^{-1}$, ascribed to Mo—O—Al bonds typical of Anderson structures, corresponds to $Mo—O_b$ modes observed in the spectrum of analog $RhMo_6$ phase [Fig. 4(a)] ($\nu Mo—O_b$ at $549\,cm^{-1}$). In addition, the presence of α-AlO(OH) in the support as a major component is confirmed by the band centered around $333\,cm^{-1}$, in agreement with the Raman pattern of crystalline α-AlO(OH) [35].

On the other hand, in the system prepared by successive impregnation, RhMo/(B), no bands corresponding to the stretching modes of Rh—O ($560\,cm^{-1}$) were found. It is also suggested that in this

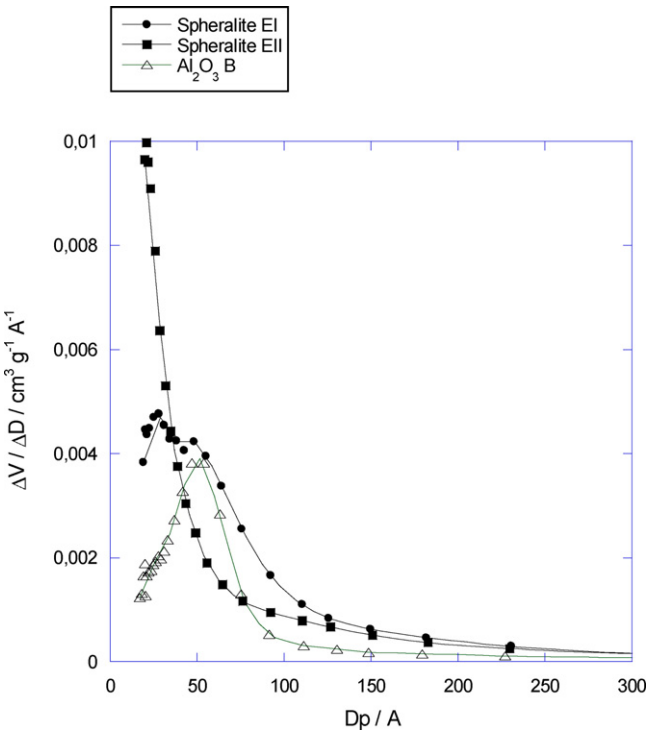

Fig. 3. Pore size distributions of the pure supports Spheralite E(I), E(II) and γ-Al_2O_3(B).

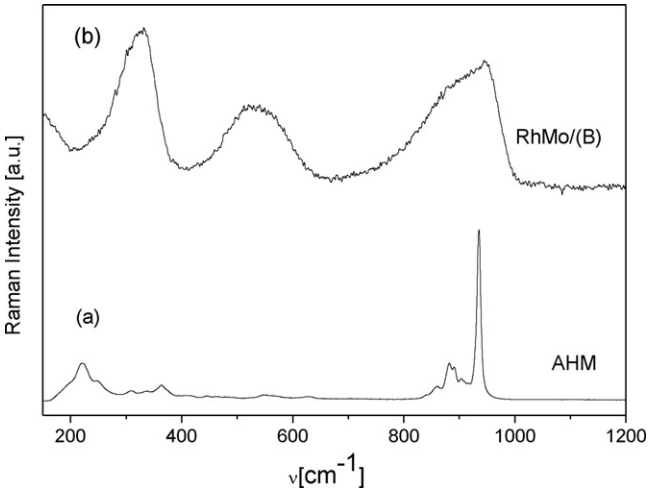

Fig. 5. Raman spectra of (a) $(NH_4)_6Mo_7O_{24}\cdot 4H_2O$ (AHM) and (b) RhMo/(B).

Table 2
Binding energies (eV) and surface composition of pure $RhMo_6$ and different supported catalysts.

Sample	$Rh3d_{5/2}$ (eV)	$Mo3d_{5/2}$ (eV)	Sample composition	
			(nRh/nMo)[a]	(nRh/nMo)[b]
$RhMo_6$	310.8	233.0	0.17	0.167
$RhMo_6$/(EI)	309.4	232.7	0.23	0.223
RhMo/(B)	309.3	232.6	1.22	0.229

[a] XPS derived values.
[b] Analytical data.

system, Rh—O—Al bands may overlap with the broad feature assigned to the Mo—O—Al stretching modes [36,37].

XPS analysis provided some insight into the chemical state and dispersion degree of the surface species both for the unsupported $RhMo_6$ compound and for the supported catalysts: $RhMo_6/Al_2O_3$[E(I)] and $RhMo/Al_2O_3$(B), Table 2.

Data for the pure $RhMo_6$ phase revealed a $Rh3d_{5/2}$ signal at 310.8 eV and a $Mo3d_{5/2}$ signal at 233.0 eV, corresponding to Rh(III) and Mo(VI), respectively. Because of the overlapping of N1s with the $Mo3p_{3/2}$ component, the state and amount of N could not be determined. The surface atomic composition nRh/nMo = 0.17, derived from the Rh/Mo intensity ratio [26], is in excellent agreement with the bulk composition, nRh/nMo = 0.167.

Both $RhMo_6/Al_2O_3$[E(I)] and conventional system $RhMo/Al_2O_3$(B) samples showed practically constant $Rh3d_{5/2}$ (309.2 ± 0.2 eV) and $Mo3d_{5/2}$ (232.4 ± 0.2 eV) binding energies that are characteristic of Rh(III) and Mo(VI), respectively (see Table 2). As for H_2 pretreated samples, although care was taken to avoid surface reoxidation during insertion into the XPS instrument, no reduced Mo and Rh species were detected. However, surface reoxidation is not expected to affect surface composition. Similar results, within experimental error, were obtained both for fresh and pretreated samples. For the $RhMo_6/Al_2O_3$ [E(I)] sample, the agreement between bulk and surface nRh/nMo atomic ratios was indicative of a uniform distribution of the $RhMo_6$ phase on the support surface. Conversely, the conventional catalyst prepared by successive impregnation of alumina B, exhibits Rh surface enrichment, as inferred from the increase of the nRh/nMo surface ratio.

The TPR technique can be an interesting method for studying the $RhMo_6$ heteropolyanion-support interaction and the influence of the Rh heteroatom on Mo reducibility [24–26,38–41]. Fig. 6 shows comparative TPR diagrams of the AHM and $RhMo_6$ bulk phases and $RhMo_6$/E(I)/(B) and RhMo/(B) fresh catalysts, whereas Table 3 collects the TPR data corresponding to the Rh and Mo reduction steps observed for the various samples.

The TPR profile of AHM (Fig. 6, curve a) consisted of a low intensity peak at about 703 K and a high intensity one at about 1033 K, corresponding to two reduction steps: $Mo(VI) \xrightarrow{(1)} Mo(IV) \xrightarrow{(2)} Mo^0$.

Table 3
TPR data corresponding to the Rh and Mo reduction steps observed for the various bulk and supported catalysts.

Sample	TPR signal (°K)		
	Rh(III)–Rh^0	Mo(VI)–Mo(IV)	Mo(IV)–Mo^0
AHM	–	703 vw	1034 vs
$RhMo_6$	550 vs	643 w	980 vw
$RhMo_6$/(EI) or (EII)	484 (480) vs	580 (660) w	–
$RhMo_6$/(B)	482 vs	604–639 w	856 w
RhMo/(B)	516 m	645 m	876 m

Ref.: m: medium, s: strong, w: weak, v: very.

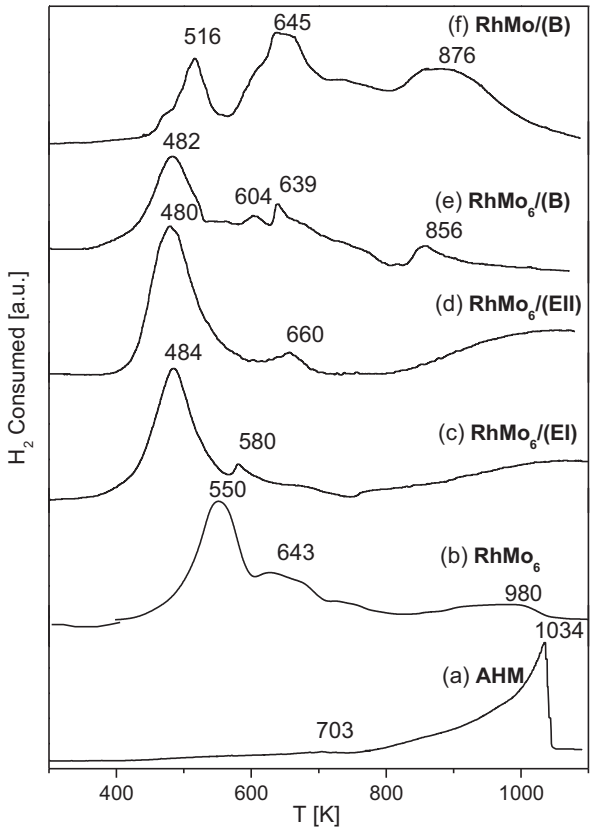

Fig. 6. TPR patterns of bulk phases and supported catalysts: (a) AHM and (b) $RhMo_6$; (c) $RhMo_6$/E(I); (d) $RhMo_6$/E(II); (e) $RhMo_6$/(B) and (f) RhMo/(B).

The profile for $RhMo_6$ species displayed an intense peak at 550 K and low intensity H_2 consumption peaks at 643 and 980 K (Fig. 6, curve b). The first peak can be related to the reduction of Rh(III) to Rh^0 and the two low intensity peaks can be assigned to the molybdenum reduction steps. The $RhMo_6$/E(I) catalyst exhibited H_2 consumption peaks at 484 and 580 K and a broad feature at about 1000 K (Fig. 6, curve c), whereas both RhMo/(B) and $RhMo_6$/(B) catalysts showed complex TPR profiles with a new contribution in the range 600–900 K (Fig. 6, curves e and f).

Dispersion of the $RhMo_6$ phase, either on E(I) or E(II) support, resulted in a promoting effect on the reduction behavior of both Rh and Mo species. The reduction temperature shifted to lower values and yielded a partial overlapping of both the contributions due to $Rh(III) \rightarrow Rh^0$ and Mo reduction steps. Likewise, the decrease in temperature of the first TPR peak of the $RhMo_6$ catalysts, if compared with the same TPR peak of the bulk phase, indicates that there was an enrichment of Rh on the surface of the catalysts, especially for support B, as demonstrated by XPS analysis.

For the [$RhMo_6$/(B)] and [RhMo/(B)] catalysts, the peaks at lower temperature are assigned to Rh reduction and the other can be assigned to Mo reduction steps. Their patterns (Fig. 6, curves e and f), are more complex than the patterns detected for the $RhMo_6$–E(I)/E(II) samples (Fig. 6, curves c and d). The TPR results confirm that the successive adsorption of Rh(III) and Mo(VI) on alumina produced the formation of X(Rh/Al)Mo_6 Anderson species and other oxides such as MoO_3 or MoO_{3-x} whose reduction temperatures lie around 900 K [24,39–41].

The high $RhMo_6$ reducibility can be associated with the reduction potential of the heteroatom [E^0 Rh(III)–Rh^0 = 0.44 V], which promotes H_2 activation. In fact, Rh(III) affects the stability of Mo(VI), whose reduction starts at lower temperature, as evidenced by high H_2 consumptions peaks centered at 550 K in the pure phase and at

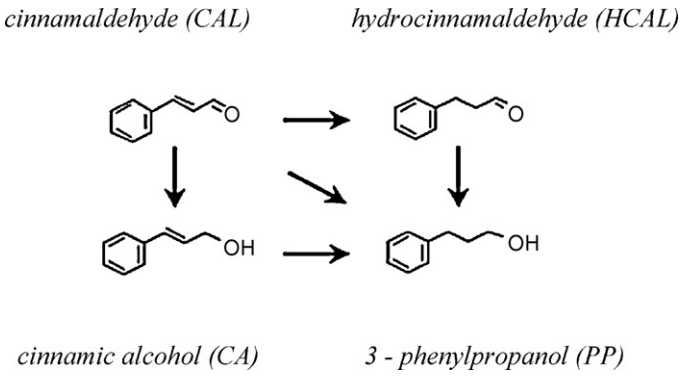

Scheme 1.

484 K in the supported ones. According to our recent investigations, this behavior is comparable to that found in other heteropolyanions of Anderson type XMo_6 [X = Cu(II), Co(III), Ni(II), Al(III)] supported on alumina [24,25,39–41]. The comparison between different phases allowed us to conclude that, in general, the reduction temperatures for the two processes $Mo(VI) \xrightarrow{(1)} Mo(IV) \xrightarrow{(2)} Mo^0$ depend mainly on the reducibility of the heteroatom. In general, when the heteroatom was less reducible, Mo(VI) became more stable.

It was also evident that the heteroatom influence on Mo reducibility depends on its redox potential according to the following order: E^0 Rh(III) > E^0 Al(III) > E^0 Mo(VI) [24,39].

3.2. Catalytic evaluation

Possible paths for the hydrogenation of cinnamaldehyde (CAL), involving the formation of cinnamic alcohol (CA, formed by hydrogenation of the C=O bond), hydrocinnamaldehyde (HCAL, formed by hydrogenation of C=C bond) and 3-phenylpropanol (PP, formed through the hydrogenation of both C=O and C=C bonds) can be observed in Scheme 1.

The chromatographic analysis indicated that cinnamaldehyde hydrogenation on our studied catalysts essentially formed HCAL, CA and PP. Catalyst composition, conversion and selectivity values after 75 min of hydrogenation of cinnamaldehyde (CAL) are listed in Table 4.

The evolution of cinnamaldehyde conversion as a function of time is shown in Fig. 7 for all the catalysts. The conversion attained with $RhMo_6$/E(I) and $RhMo_6$/E(II) catalysts was significantly higher than the corresponding values for RhMo/(B) and $RhMo_6$/(B). After ca. 60 min reaction time, more than 60% CAL had been converted in $RhMo_6$/E(I) and $RhMo_6$/E(II) catalysts.

On the other hand, B-supported catalysts showed a conversion profile corresponding to a catalyst of very low activity. Initial CAL conversion rates (r_0, μmol s^{-1}) were calculated by extrapolation to zero time and gathered in Table 5 with the Rh atoms number, Rh dispersion as H/Rh and TOF values [42,43]. The r_0 and TOF for

Table 4
Composition (adsorbed Mo and Rh, wt%); conversion (%) and selectivity (%) for all catalysts on the hydrogenation of cinnamaldehyde (CAL) to hydrocinnamaldehyde (HCAL), cinnamic alcohol (CA) and 3-phenyl propanol (PP).

Catalyst	C_a^{Mo} (%)	C_a^{Rh} (%)	Conversion[a] (%)	Selectivity (%)[b]		
				HCAL	CA	PP
$RhMo_6$/(EI)	6.0	1.5	79.0	100.0	0.0	0.0
$RhMo_6$/(EII)	6.7	1.5	59.0	100.0	0.0	0.0
$RhMo_6$/(B)	5.7	1.4	16.0	94.0	0.0	6.0
RhMo/(B)	6.0	1.0	11.0	90.0	10.0	0.0

[a] Conversion at 75 min reaction.
[b] Selectivity at 15% conversion, except for RhMo/(B) calculated at 10% conversion.

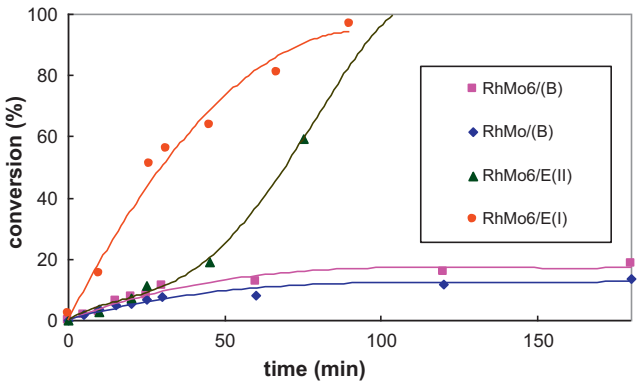

Fig. 7. Cinnamaldehyde conversion as a function of time for $RhMo_6$/E(I); E(II); (B) and RhMo/(B) catalysts.

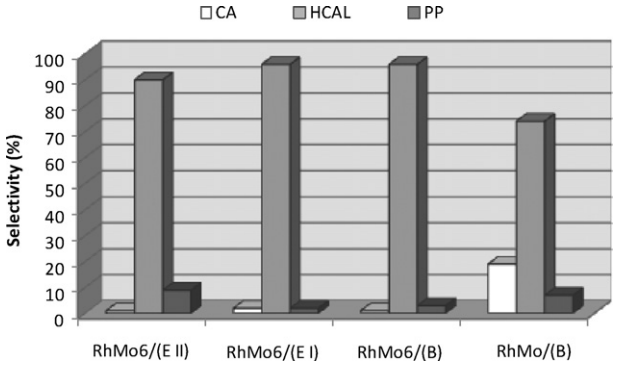

Fig. 8. Selectivity (%) at 55% conversion for the cinnamaldehyde hydrogenation reaction for $RhMo_6$/(EI, EII and B) and RhMo/(B) catalysts.

$RhMo_6$/E(I) are about one order of magnitude higher than those of the rest of the catalysts studied. Although $RhMo_6$/E(II) showed the highest activity at 75 min, its values of TOF and dispersion of Rh were comparable to those of catalysts supported on alumina (B).

The product selectivity at 15% conversion of CAL is listed in Table 4 (except for RhMo/(B) measured at 10% conversion). The main reaction product with the four catalysts was HCAL (as seen in Fig. 8), thus indicating that they selectively catalyze the hydrogenation of the C=C bond. To explain the behavior related to selectivity, we must consider that the proximity between the Rh and Mo, in addition to the stoichiometry and structure of the heteropolyanion, could lead to the oxidative stabilization of small aggregates of Rh. As a result, the interaction of Rh with carbonyl from cinnamaldehyde, favors the formation of HCAL. These results are in agreement with those reported by the extensive work of Lowenthal et al. about chemisorption of H and CO for various systems of Rh and Mo supported on both silica and alumina [21].

These studies have showed that a close proximity of Mo and Rh lead to both oxidative and kinetic stabilization of small aggregates of Rh and the coexistence of species $Rh^{\delta+}$ and MoO_x. Nevertheless,

Table 5
Rh number atoms, initial rate of CAL conversion, Rh dispersion as H/Rh and TOF calculated from [CAL] μmoles s^{-1}/Rh surface atoms.

Catalyst	Rh atoms[a] ($\times 10^{19}$)	Rh dispersion (H/Rh)	Initial rate (CAL μmol s^{-1})	TOF ($\times 10^{-3}$)
$RhMo_6$/E(I)	1.75	0.50	2.45	168
$RhMo_6$/E(II)	1.75	0.35	0.502	49
$RhMo_6$/(B)	1.64	0.34	0.370	40
RhMo/(B)	1.17	0.30	0.256	44

[a] In 0.200 g of sample.

with RhMo/(B) catalyst a certain level of CA was obtained (10%). In general, systems based on $RhMo_6$ showed a different catalytic performance in the hydrogenation of cinnamaldehyde if they are compared to the RhMo/(B) catalyst based on Rh and AHM.

Taking into account that XRD did not indicate the presence of structures containing Rh and/or Mo in the supported catalysts, it is possible to suggest that Rh species are present as small metallic particles that cannot be observed by XRD. In addition, TPR results for $RhMo_6$ systems showed the Rh reduction at low temperature. This effect may also indicate that reduced species are dispersed as small particles weakly interacting with the support and therefore, the selectivity results can be explained in terms of a particle size effect.

According to the classical paper of Richard et al. [44], large particles lead to the unsaturated alcohol preferentially, whereas small particles lead to the saturated aldehyde. Besides, steric factors related to the molecule to be reduced cannot be discarded, and thus, the stiffness of the cinnamaldehyde molecule (where the phenyl ring is conjugated with C=C and C=O bonds) favors its adsorption via the C=C bond on small particles and the C=O bond on large particles [10].

Then, the selectivity to CA obtained with the RhMo/(B) catalyst may be explained as a consequence of the effect of both Mo(VI) and Rh(III). In fact, the RhMo/(B) (Fig. 6(f)) TPR showed that the reduction peaks appear at higher temperature than those of the other catalysts and thus the amount of non-reduced Rh species at the temperature employed in the reduction pretreatment of our catalysts (623 K) could be higher than for the other catalysts. Besides, XPS data revealed a surface enrichment in $Rh^{\delta+}$ species, which could be responsible for C=O bond polarization. In addition, the effect of Mo(VI) may have caused the activation of the C=O bond, facilitating the hydrogen transfer from adjacent Rh sites.

On the other hand, the comparison between the three catalysts based on supported Anderson phase, $RhMo_6$/E(I)/E(II) and/(B), indicates that textural differences of the support seem to cause a significant effect on their catalytic behavior. In fact, BJH analysis of adsorption data on the three supports shows that the *cumulative pore areas* for mesopores (below 30 Å) are 150, 50 and 20 $m^2\,g^{-1}$ for E(II), E(I) and alumina (B), respectively. Maybe this high fraction (about 50%) of the BET surface area of the support E(II) is difficult to be reached by Anderson phase during the preparation, whereas alumina E(I) exhibits a more favorable pore size distribution with only 20% of the total BET surface area entrapped in narrow mesopores (see Fig. 3). The observed differences in both the dispersion of the metallic phase and the TOF values may be assigned to the different textural characteristics of these two supports.

Finally, it is possible to suggest that the preferentially C=C hydrogenation of catalysts based on $RhMo_6$ species depends mainly on the nature of the heteropolyanion that provokes a reduction in the ability of both metals needed for generating the selective hydrogenation of CAL. An additional advantage in the use of the heteropolyanion as catalyst precursor is the smallest amount of Rh and the avoidance of sintering.

4. Conclusions

In general, systems based on $RhMo_6$ show a better catalytic performance in the hydrogenation of cinnamaldehyde to hydrocinnamaldehyde than the catalyst prepared by successive impregnation.

Raman and XPS spectroscopies detected typical features corresponding to the presence of Anderson type structures on the surface of all catalysts, including the catalyst prepared by successive impregnation of Rh(III) and Mo(VI) salts.

The temperature programmed reduction (TPR) technique revealed that Rh species induce Mo(VI) reducibility at lower temperatures in the catalysts as well as in the pure phase, confirming the coexistence of $Rh^{\delta+}$ and MoO_x, species, and thus the oxidative stabilization of small Rh aggregates for the heteropolyanion structure.

This study confirms that the heteropolyanion-support interaction produces an active surface with an ordered distribution of Rh and Mo in the support causing a synergic effect that favors the catalytic activity.

References

[1] P. Gallezot, D. Richard, Catal. Rev. Sci. Eng. 40 (1998) 81.
[2] J. Kijenski, P. Winiarek, Appl. Catal. A: Gen. 193 (2000) L1–L4.
[3] F. Delbecq, P. Sautet, J. Catal. 152 (1995) 217.
[4] I. Kroschwitz (Ed.), Kirk-Othmer, En. of Chem. Tech., vol. 6, 4th ed., Wiley, New York, 1992, p. 349.
[5] S. Narayanan, Bull. Catal. Soc. India 2 (2003) 107.
[6] A.M.C.F. Castelijns, J.M. Hogeweg, S.P.J.M. van Nispen, PCT Int. Appl. WO 96/11898 Al (April 25, 1996) 14 pp.
[7] A.M.C.F. Castelijns, J.M. Hogeweg, S.P.J.M. van Nispen, PCT Int. Appl., US Patent 5,811,588 (September 22, 1998) pp. 6.
[8] A. Muller, J. Bowers, WO Patent WO 99/08989 (February 25, 1999) to First Chemical Corporation.
[9] G.F. Santori, M.L. Casella, O.A. Ferretti, J. Mol. Catal. A: Chem. 186 (2002) 223.
[10] M. Lashdaf, A.O.I. Krause, M. Lindblad, M. Tiitta, T. Venäläinen, Appl. Catal. A: Gen. 241 (2003) 65.
[11] J. Breen, R. Burch, J. Gomez-Lopez, K. Griffin, M. Hayes, Appl. Catal. A: Gen. 268 (2004) 267.
[12] P. Reyes, C. Rodriguez, G. Pecchi, J.L. Fierro, Catal. Lett. 69 (2000) 27.
[13] P.N. Rylander, Catalytic Hydrogenation in Organic Syntheses, Academic Press, New York/San Francisco/London, 1979, p. 78.
[14] A. Giroir-Fendler, D. Richard, P. Gallezot, Stud. Surf. Sci. Catal. 41 (1988) 171.
[15] Y. Zhang, S. Liao, Y. Xu, D. Yu, Appl. Catal. A: Gen. 192 (2000) 247.
[16] J.-P. Tessonnier, L. Pesant, G. Ehret, M.J. Ledoux, C. Pham-Huu, Appl. Catal. A: Gen. 288 (2005) 203.
[17] Y. Kume, K. Qiao, D. Tomida, C. Yokoyama, Catal. Commun. 9 (2008) 369–375.
[18] V. Ponec, Appl. Catal. A: Gen. 222 (2001) 31.
[19] B.M. Reddya, G.M. Kumara, I. Ganesh, A. Khan, J. Mol. Catal. A: Chem. 247 (2006) 80.
[20] B. Coq, F. Figueras, J. Mol. Catal. A: Chem. 173 (2001) 117.
[21] E.E. Lowenthal, L.F. Allard, M. Te, H.C. Foley, J. Mol. Catal. A: Chem. 100 (1995) 129–145.
[22] N. Mizuno, M. Misono, Chem. Rev. 98 (1998) 199.
[23] C.I. Cabello, I.L. Botto, H.J. Thomas, Appl. Catal. A 197 (2000) 79.
[24] C.I. Cabello, I.L. Botto, F. Cabrerizo, M. González, H. Thomas, Adsorpt. Sci. Technol. 18 (7) (2000) 591.
[25] C.I. Cabello, I.L. Botto, M. Muñoz, H. Thomas, Stud. Surf. Sci. Catal. 143 (2002) 565–573.
[26] C.D. Wagner, L.E. Davis, M.V. Zeller, J.A. Taylor, R.H. Raymond, L.H. Gale, Surf. Interface Anal. 3 (1981) 211.
[27] Brunauer, Emmett and Teller (BET) method, in: J.R. Anderson, K.C. Pratt (Eds.), Introduction to Characterization and Testing of Catalysts, Academic Press, Australia, 1985.
[28] E.P. Barrett, L.G. Joyner, P.P. Halenda, J. Am. Ceram. Soc. 73 (1951) 373.
[29] B.J. Lippens, J.H. de Boer, J. Catal. 4 (1965) 319.
[30] W.D. Harkins, G. Jura, J. Am. Ceram. Soc. 66 (1944) 1366.
[31] L. Gurvitsch, J. Phys. Chem. Soc. Russ. 47 (1915) 805.
[32] J.E. Benson, M. Boudart, J. Catal. 4 (1965) 704.
[33] C.I. Cabello, M. Muñoz, I.L. Botto, E. Payen, Thermochim. Acta 447 (2006) 22.
[34] L. Le Bihan, P. Blanchard, M. Fournier, J. Grimblot, E. Payen, J. Chem. Soc., Faraday Trans. 94 (7) (1998) 937.
[35] C.J. Doss, Phys. Rev. B 48 (1993) 15626.
[36] S. Musić, A. Šarić, S. Popović, M. Ivanda, J. Mol. Struct. 221 (2009) 924–926.
[37] C.T. Williams, E.K.-Y. Chen, C.G. Takoudis, M.J. Weaver, Phys. Chem. J. B102 (1998) 4785.
[38] C.I. Cabello, I.L. Botto, H.J. Thomas, Thermochim. Acta 232 (2) (1994) 183.
[39] I.L. Botto, C.I. Cabello, G. Minelli, M. Occhiuzzi, Mater. Chem. Phys. 39 (1) (1994) 21–28.
[40] I.L. Botto, C.I. Cabello, H.J. Thomas, Mater. Chem. Phys. 47 (1) (1997) 37.
[41] I.L. Botto, C.I. Cabello, H.J. Thomas, D. Cordischi, G. Minelli, P. Porta, Mater. Chem. Phys. 62 (3) (2000) 254–262.
[42] A. Merlo, B. Machado, V. Vetere, J.L. Faria, M. Casella, Appl. Catal. A: Gen. 383 (2010) 43.
[43] L. Mercadante, G. Neri, C. Milone, A. Donato, S. Galvagno, J. Mol. Catal. A: Chem. 105 (1996) 93.
[44] A. Giroir-Fendler, D. Richard, P. Gallezot, Catal. Lett. 5 (1990) 175.